A&A 463, 579–587 (2007)
DOI: 10.1051/0004-6361:20066303

Astronomy & Astrophysics

The Pleiades eclipsing binary HD 23642 revisited⋆,⋆⋆

M. A. T. Groenewegen[1], L. Decin[1,⋆⋆⋆], M. Salaris[2], and P. De Cat[3]

[1] Instituut voor Sterrenkunde, Celestijnenlaan 200D, 3001 Leuven, Belgium
e-mail: groen@ster.kuleuven.be
[2] Astrophysics Research Institute, Liverpool John Moores University, Twelve Quays House, Egerton Wharf, Birkenhead CH41 1LD, UK
[3] Koninklijke Sterrenwacht, Ringlaan 3, 1180 Brussels, Belgium

Received 28 August 2006 / Accepted 31 October 2006

ABSTRACT

Context. HD 23642 is the only known eclipsing binary in the Pleiades, and therefore of importance in determining the distance to this cluster.
Aims. To use new photometric and spectroscopic data in combination with existing data in the literature in order to improve the determination of the parameters of the system, its distance and reddening.
Methods. New photometric and spectroscopic data are presented for HD 23642. The spectroscopic data are "spectrally disentangled" using the KOREL code. The new and literature photometric and radial velocity data are simultaneously analysed using the FOTEL code to obtain the orbital solution and derive the fundamental parameters of the two stars. The distance and reddening are determined by fitting 7-colour Geneva, B, V and Strömgren colours, and considering surface-brightness relations for the two components in $(B-V)$ and Strömgren c_1-index.
Results. The preferred distance is 138.0 ± 1.5 pc for a reddening of $E(B-V) = 0.025 \pm 0.003$. The reddening value is larger than the 0.012 adopted in the recent works on this stars by Munari et al. (2004) and Southworth et al. (2005), and smaller than other values in the literature for the cluster reddening. The distance is in agreement with other recent works on the distance to the Pleiades. A comparison with evolutionary models suggests that the inclusion of convective core overshoot gives a much better fit to the empirical mass-radius relationship obtained from the binary analysis. Both this comparison and the "spectral disentangling" are consistent with HD 23642 having [Fe/H] = +0.06, a value determined by the most recent spectroscopical analyses of Pleiades stars.

Key words. stars: distances – binaries: eclipsing – stars: individual: HD 23642 – stars: fundamental parameters – open clusters and associations: individual: Pleiades

1. Introduction

HD 23642 (HIP 17704; RA = $3^h47^m29.45^s$ Dec = $+24°17'18.04''$) is a member of the Pleiades and was discovered to be a double-lined spectroscopic binary by Pearce (1957) and Abt (1958). Griffin (1995) combined the radial velocity data from these two papers to derive an improved period and orbit. Abt & Levato (1978) determined a spectral type of A0Vp(Si)+Am.

Giannuzzi (1995) used this system to derive a distance modulus (DM) of 5.61 ± 0.26 (assuming an age of 150 Myr). At that time, the eclipsing nature was unknown and he estimated the colours of the two components by requiring that both lie on the same adopted isochrone.

The interest in this system rose when Torres (2003) discovered shallow eclipses using the Hipparcos epoch photometry. He obtained four high-resolution spectra and combined the derived radial velocities (RVs) with those by Pearce (1957) and Abt (1958) to obtain a spectroscopic orbit. The actual values of the RVs obtained by Torres remain unpublished.

Munari et al. (2004, hereafter M04) obtained high-resolution spectra at 5 epochs, and of order 500 and 400 photometric data points in V and B. They analysed the light-curve (LC) and RV curve using a recent version of the Wilson-Devinney (WD) code (Wilson & Devinney 1971) to obtain the fundamental parameters of the system. The distance they derived was 132 ± 2 pc.

The spectroscopic and photometric datasets obtained by M04 were re-analysed by Southworth et al. (2004, 2005, hereafter S05) with the codes EBOP (Etzel 1975, 1981; Popper & Etzel 1981) and SBOP to find a distance near 139 pc. The difference w.r.t. the M04 result is ascribed by them partly to the smaller radii they find and partly to the adopted luminosity and absolute magnitude of the Sun. In fact, they claim that there is an inconsistency between the Solar luminosity and absolute magnitude adopted in the WD-code and in the bolometric corrections (BCs) adopted by Munari et al., and that, taking the masses, radii and effective temperatures in M04 the distance should be 135.5 ± 2.3 pc. S05 also use surface-brightness (SB) relations to independently find a distance of 139 pc. Their finally adopted distance to the Pleiades is 139.1 ± 3.5 pc (for a reddening of $E(B-V) = 0.012$) and is based on a SB relation.

⋆ Table 3 is only available in electronic form at the CDS via anonymous ftp to cdsarc.u-strasbg.fr (130.79.128.5) or via http://cdsweb.u-strasbg.fr/cgi-bin/qcat?J/A+A/463/579

⋆⋆ Based on observations obtained with the 1.2 m Flemish Mercator Telescope, at La Palma (Spain) and on observations with the 1.2 m Swiss Euler Telescope at La Silla (Chile).

⋆⋆⋆ Postdoctoral fellow of the Fund for Scientific Research, Flanders (FWO).

In the present paper new spectroscopic and photometric data are presented (Sect. 2). The "spectral disentangling" of the spectra is described in Sect. 2, and the fitting of the component spectra with MARCS model atmospheres is described in Sect. 3. Section 4 details the analysis of the photometric and RV data to obtain the orbital solution and fundamental parameters of the two stars. Section 5 discusses the distance to the object by comparing synthetic photometry to the observations, and also considering SB relations. Section 6 compares the radii of both components to recent isochrones. Section 7 concludes the paper.

2. The data

2.1. Spectroscopy and "spectral disentangling"

High-resolution spectra were obtained on 11 different occasions between 20 December 2002 and 11 August 2004 using the CORALIE spectrograph at the 1.2 m EULER telescope located at the La Silla observatory, Chile. This is 2-fibre-fed echelle spectrograph (2″ fibres on the object and sky, respectively), which covers the 3880 to 6810 Å region in 68 orders with a spectral resolution of about 50 000. Exposure times are between 25 and 40 min, resulting in a *S/N* of order 150. During each night, several exposures with a tungsten lamp are taken to measure the relative pixel sensitivity variation of the CCD. A Thorium-Argon lamp is observed at the beginning and end of the night for wavelength calibration.

Right after the science exposure is taken, the standard pipeline reduction is carried out which is based on scripts written in TACOS-INTER (software developed by the Observatory of Geneva, Baranne 1996). In this reduction scheme only the last tungsten exposure prior to the science exposure is used to measure the flat-field. To reduce the amount of noise, we optimised the pipeline reduced spectra such that an average of all the tungsten exposures (about 10) of the considered night is used for the flat-fielding instead. The spectra are also corrected for the blaze and every echelle order is re-binned in steps of 0.018 Å. The wavelength scale is converted to the heliocentric one.

Seventeen echelle orders are considered, chosen predominantly as being the most suitable to fit the model atmospheres to the component spectra as described in Sect. 3. They are listed in Table 1 for reference. For those orders, cosmic rays are removed in every spectrum by visual inspection. Finally, the spectra are continuum normalised by interactively selecting continuum points. To optimise this, MARCS model atmospheres, to be described in Sect. 3, with appropriate parameters for the components effective temperatures, stellar radii and radial velocities, are used to compute approximate synthetic continuum-normalised spectra in the wavelength region of each order. The output of the data reduction process are hence 17 continuum normalised spectra for each observing date.

KOREL (Hadrava 1995, 2004b), and the auxiliary program PREKOR[1] are then used to separate the spectra into those of the two components separately (usually called "spectral disentangling"). For each order, PREKOR is used to select the exact wavelength region by specifying a start wavelength and a velocity step (typically 3.5 to 6.0 km s^{-1}). The input spectra are then re-binned to exactly 512 wavelength points and put into the format needed as input to KOREL.

KOREL is run keeping the period fixed and with zero eccentricity, allowing the time of primary minimum, one semi-amplitude and the mass-ratio to vary. The parameters of the Earths' orbit (period, eccentricity, mass ratio Earth/Sun) are included to allow the "spectral disentangling" of telluric lines.

The output of KOREL are the relevant parameters of the orbit (T_0, K_1 and q in this case), the radial velocities of the two components and the disentangled spectra of both components in the reference frame of the binary system.

Table 2 lists the observation date and the heliocentric velocities relative to the systemic velocity, as the spectral disentangling is not sensitive to a constant velocity shift. For every observation date RVs are available for each of the 17 selected orders and the values quoted in Table 2 are the median values. From the scatter of the RV over the orders, the typical errors are estimated to be 0.9 and 1.5 km s^{-1} for the primary and secondary, respectively.

In Sect. 3 the disentangled spectra are fitted with model atmospheres. For that application it is important that the spectra included in the disentangling are outside of the eclipses. For that reason the procedure described above is repeated excluding the spectra taken at HJD 52 631.6089 (ϕ = 0.735), 52 636.6055 (ϕ = 0.765) and 52 983.6570 (ϕ = 0.778) which are all close to the secondary eclipse.

[1] See `http://www.asu.cas.cz/~had/korel.html`

Table 1. Spectral orders that have been considered and the wavelength range.

Order	$\lambda_{\rm min}$ (Å)	$\lambda_{\rm max}$ (Å)
03	3927	3943
14	4230	4257
19	4390	4415
20	4410	4439
21	4438	4466
22	4465	4506
23	4506	4546
24	4545	4579
28	4695	4719
35	4949	4989
37	5027	5061
40	5156	5201
41	5192	5245
46	5423	5470
60	6221	6261
62	6330	6383
63	6392	6441

Table 2. Heliocentric radial velocities of HD 23642, *relative to the systemic velocity*.

HJD (+2 400 000.0)	RV_1 (km s^{-1})	RV_2 (km s^{-1})
52 629.6190	88.8	−127.0
52 630.6098	−48.0	68.0
52 631.6089	−9.5	13.1
52 632.6024	63.6	−90.9
52 633.6162	−94.5	135.0
52 636.6055	10.3	−13.9
52 983.6570	18.1	−25.1
52 987.6453	−80.6	114.5
52 993.6322	49.0	−70.7
53 224.9338	39.0	−55.7
53 229.9384	57.2	−82.0

Typical errors, based on the scatter between the radial velocities from the different echelle orders, are 0.9 and 1.5 km s^{-1} for the primary and secondary, respectively.

Table 3. Geneva photometry obtained for HD 23642.

HJD (+2 400 000.0)	Quality Flag	V	$U-B$	$V-B$	$B1-B$	$B2-B$	$V1-B$	$G-B$
52 925.68325	2	6.827	1.424	0.878	0.900	1.481	1.579	2.051
52 925.69350	2	6.840	1.423	0.877	0.903	1.482	1.573	2.048
52 925.70311	2	6.857	1.423	0.878	0.901	1.483	1.579	2.051
52 925.73409	2	6.913	1.426	0.875	0.903	1.482	1.573	2.047
52 925.73934	2	6.914	1.424	0.873	0.902	1.481	1.573	2.046
52 925.74466	2	6.922	1.422	0.874	0.902	1.480	1.573	2.045
52 926.71589	2	6.806	1.427	0.872	0.895	1.475	1.573	2.043
52 926.73755	2	6.820	1.427	0.873	0.899	1.482	1.577	2.047
52 928.69695	2	6.816	1.427	0.880	0.899	1.483	1.581	2.055
52 928.71119	2	6.816	1.423	0.879	0.899	1.486	1.581	2.053
52 931.71328	2	6.815	1.429	0.881	0.902	1.484	1.584	2.052
52 931.73387	2	6.813	1.426	0.883	0.901	1.484	1.584	2.059
52 945.41427	3	6.881	1.417	0.867	0.902	1.474	1.571	2.038
52 945.41984	3	6.893	1.420	0.870	0.901	1.479	1.568	2.039
52 945.42507	3	6.902	1.418	0.866	0.902	1.473	1.564	2.036
52 945.43032	3	6.917	1.426	0.863	0.905	1.474	1.567	2.038
52 945.43556	3	6.914	1.420	0.863	0.902	1.473	1.567	2.035
52 945.44079	3	6.919	1.418	0.868	0.900	1.476	1.567	2.038
52 945.44601	3	6.921	1.419	0.865	0.901	1.475	1.568	2.040
52 945.45125	3	6.916	1.424	0.865	0.901	1.473	1.568	2.043
52 945.45651	3	6.914	1.424	0.867	0.904	1.473	1.570	2.039
52 945.46178	3	6.905	1.420	0.865	0.900	1.473	1.567	2.037
52 945.46706	3	6.900	1.424	0.868	0.900	1.474	1.569	2.041
52 945.47233	3	6.890	1.425	0.871	0.901	1.476	1.571	2.042
52 945.47760	3	6.875	1.424	0.866	0.902	1.473	1.570	2.036
52 945.48285	3	6.868	1.428	0.874	0.904	1.480	1.574	2.045
52 945.48808	3	6.857	1.424	0.872	0.902	1.477	1.572	2.042
52 945.49331	3	6.847	1.423	0.873	0.901	1.477	1.574	2.044
52 945.49857	3	6.840	1.428	0.874	0.903	1.480	1.579	2.049
52 945.50381	3	6.834	1.426	0.872	0.903	1.476	1.575	2.045

First entries only. Complete table is available in electronic form at the CDS.

2.2. Photometry

Geneva $V, B, U, B1, B2, V1, G$ photometry was obtained on various occasions between 12 October 2003 and 29 August 2004 using the P7 photometer attached to the 1.2 m MERCATOR telescope on the island of La Palma, Spain. P7 is a two-channel photometer (object and sky) for quasi-simultaneous 7-band measurements. A filter-wheel and chopper ensure that the photomultiplier observes object and sky 4 times per second. Standard stars are observed regularly, and the final reduction is done by the photometric group of the Geneva Observatory, which is not only based on the observations of this particular program but based on *all* P7 measurements. Table 3 lists the 211 data points. The table includes the quality flag[2] that had to be ≥2 for inclusion in the lightcurve analysis.

3. Determination of the effective temperatures

The synthetic spectra used in this study have been generated using model photospheres calculated with the MARCS code (Gustafsson et al. 1975), and further improved by, e.g. Plez et al. (1992), Jørgensen et al. (1992) and Edvardsson et al. (1993). More details on the code and used line lists can be found in Decin et al. (2000, 2004)

A grid of model atmospheres is calculated with parameters $\log g = 4.0$ and 4.3, [Fe/H] = 0.0 and +0.10, and for the primary $T_{\rm eff}$ = 9500 and 10 500 K, and for the secondary $T_{\rm eff}$ = 7250 and 8000 K. The wavelength runs from 3000−7000 Å and covers the range observed with the CORALIE spectrograph.

The model that is fitted to the component spectra simultaneously has 9 free parameters: the effective temperatures of the primary and secondary (T_1, respectively T_2), $\log g$ of the secondary ($\log g_2$; the gravity of the primary being fixed by the known difference ($\log g_1 - \log g_2$) from the RV and LC analysis), the metallicity Z ($=10^{\rm [Fe/H]}$, assumed the same for both components), the rotational velocities for the primary and secondary ($V_{\rm rot,1} \sin i$, $V_{\rm rot,2} \sin i$), the continuum shifts for the two components (s_1, s_2, related to possible shifts in the individual continua after the spectral disentangling), and the systemic velocity (V_γ).

For a given set of parameters, (1) the primary and secondary continuum and absolute flux are calculated by linear interpolation in $\log g$, $\log T_{\rm eff}$ and Z; (2) the wavelength scale is redshifted by the systemic velocity; (3) the absolute and continuum fluxes are rotationally broadened; and (4) re-binned to the observed wavelength points. No instrumental broadening was applied as it turned out to be negligible (about 6 km s^{-1}) compared to the rotational broadening. It was verified by interpolating a model with $T_{\rm eff}$ = 9000 and 9750 K to 9250 K, and comparing it directly to the corresponding MARCS model that the linear interpolation predicts fluxes correct to better than 5% in the lines.

For the primary, the ratio of the continuum fluxes is calculated under the assumption of spherical stars:

$$C_1(\lambda) = R_1^2\ F_1^{\rm cont} / (R_1^2\ F_1^{\rm cont} + R_2^2\ F_2^{\rm cont}), \quad (1)$$

with R_1 and R_2 the (relative) radii of the two components, known from the LC analysis (see next section), $F_1^{\rm cont}$ the continuum flux of the primary and $F_2^{\rm cont}$ the continuum flux of the secondary,

[2] This quality flag is part of the Geneva system photometry output (see e.g. Rufener 1988) and is a number between 0 ("risk of error") and 4 ("data of exceptional quality").

Table 4. Derived effective temperatures.

Model/variable	T_1 (K)	T_2 (K)	
$Z = 1.15$	9950 ± 370	7640 ± 380	Standard model
$Z = 1.0$	9880 ± 380	7610 ± 390	
$Z = 0.87$	9780 ± 400	7570 ± 390	
$Z = 1.10 \pm 0.29$	10 020 ± 600	7670 ± 340	Z was fitted

The Standard model has parameter values: $Z = 1.15$, $V_\gamma = 5.5$ km s^{-1}, $V_{\rm rot,1} = 36.5$ km s^{-1}, $V_{\rm rot,2} = 31.9$ km s^{-1}.

both provided by the MARCS models. Finally, the normalised synthetic spectrum is calculated:

$$NS_1(\lambda) = ((F_1/F_1^{\rm cont}) - 1.0)\, C_1 + 1.0 + s_1, \quad (2)$$

with F_1 the absolute flux also provided by the MARCS models. Similarly C_2 and NS_2 are determined for the secondary. NS_1 and NS_2 can be directly compared to the output of KOREL. This comparison is done is a χ^2-sense. The error attributed to all wavelength points (per order) is taken to be the rms in the KOREL output spectrum for the telluric lines, after these lines (if present) have been removed in one iteration of sigma-clipping.

The minimisation of the parameters is done using the MRQMIN routine (using the Levenberg-Marquardt method) from Press et al. (1992). Every order is individually fitted, and in a first run all 9 parameters are allowed to vary. The poorest constrained parameters are the $\log g_2$ value (3.9 ± 0.5), and the metallicity ($Z = 1.03 \pm 0.35$). The error estimate comes from the scatter in the parameter values from the fits to the different orders. The value for the spectroscopically derived gravity is – formally – consistent with the very precise Newtonian value derived from the mass and radius from the orbital solution (4.231 ± 0.024) and is therefore fixed to that value in the second run. As the rotational velocities are relatively small, no correction to the Newtonian gravity is needed to determine the optimum value for the spectroscopic gravity (cf. Fitzpatrick & Massa 2005, for B-stars).

The systemic velocity and rotational velocities are very well determined (5.5 ± 1.0, 36.5 ± 0.8, and 31.9 ± 1.2 km s^{-1}, respectively) and are fixed to these values in the second run. The systemic velocity derived in this way is in excellent agreement with the value of 5.42 ± 0.12 km s^{-1} derived by FOTEL (see next section) when fitting the RV curve using only the data in Table 2.

In the second run the number of parameters is thus reduced to five (T_1, T_2, Z, s_1, s_2). The median values and the rms around the median over the 17 orders are $T_1 = 10\,020 \pm 600$ K, $T_2 = 7670 \pm 340$ K, and $Z = 1.10 \pm 0.29$ (see Table 4).

Recently, Boesgaard (2005) determined a mean value of [Fe/H] = +0.06 ± 0.02 (i.e. $Z = 1.15 \pm 0.05$) based on high-resolution spectra of 20 late-F and early-G dwarfs in the Pleiades, which is slightly higher than the value of −0.03 ± 0.02 (i.e. $Z = 0.93 \pm 0.04$) derived previously by Boesgaard & Friel (1990), but is consistent with [Fe/H] = +0.06 ± 0.05 obtained by King et al. (2000). Table 4 lists the derived temperatures when the metallicity is fixed at [Fe/H] = +0.06 (from now on the metallicity adopted in the standard model), 0.0, and −0.06. As one might expect, the best fitting temperatures decrease slightly when lowering the metallicity, due to the lower opacity, but the changes are always well within the error bars in a single determination. The error due to fixing V_γ, $V_{\rm rot,1}$ and $V_{\rm rot,2}$ has been estimated by changing the values by their 1σ error bar and repeating the analysis. The effect is not significant compared to the error bar already listed in Table 4 based on the scatter between the fit over the different spectral orders.

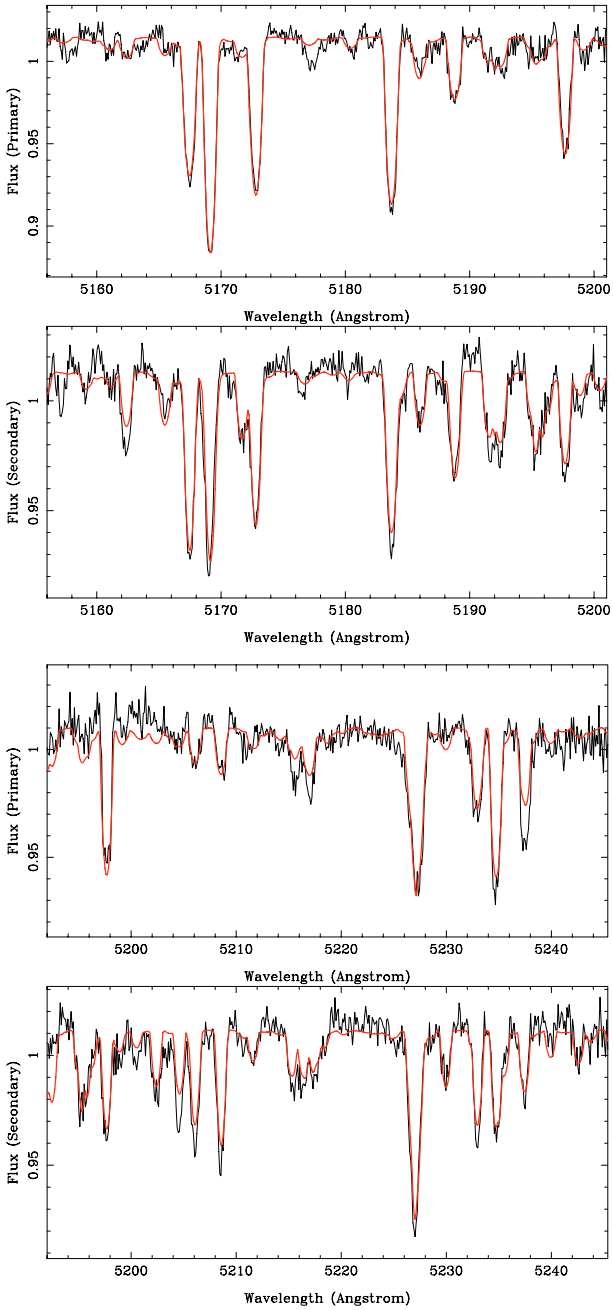

Fig. 1. Representative normalised disentangled spectra of the primary (*top*) and secondary (*bottom*), and the MARCS model fit to it, for two of the spectral orders fitted.

4. Orbital solution

The RV and LC were independently analysed using the codes FOTEL (Hadrava 1990, 2004a)[3] and PHOEBE (Prša & Zwitter 2005)[4], which is based on the WD code. Because of its closeness in concept to KOREL, FOTEL was used as the primary code, while PHOEBE was used as a check.

The RV data was taken from the present paper (Table 2), M04, Pearce (1957, only his higher quality "IS" data) and

[3] See `http://www.asu.cas.cz/~had/fotel.html` (FOTEL3 version of 29 October 2003). An apparent bug in the calculation of the reflection effect was corrected.

[4] See `http://www.fiz.uni-lj.si/phoebe/index.html` (version 0.26).

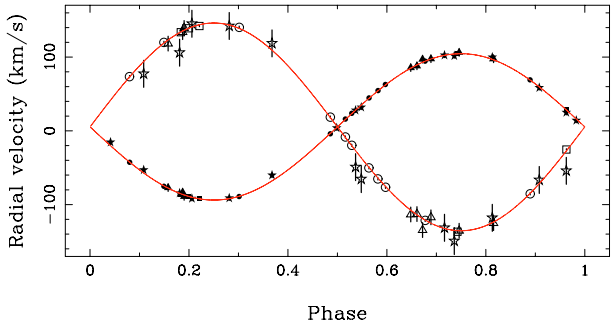

Fig. 2. Observed radial velocity curve for the primary (closed symbols) and the secondary (open symbols). Present work (circles), M04 (squares), Abt (5-pointed stars), Pearce (triangles). The fit to the data is shown by the lines. Error bars for the data points from M04 and the present work are smaller than the symbol size.

Abt (1958). The measurements of the primary and secondary were assigned error bars of 5.0 and 10.0 km s^{-1}, respectively, 3.0 and 17.0 km s^{-1} for the Pearce, and Abt data, based on information in the original papers and the discussion in Griffin (1995) and Torres (2003). The Munari et al. and Abt data were shifted by, respectively, −0.8 and +1.1 km s^{-1}.

The photometric data analysed comes from the present paper, B and V from M04, and HIPPARCOS data.

Linear limb-darkening coefficients have been interpolated using the tables in Claret (2000, 2003)[5].

The results of the LC and RV curve fitting using the two codes are listed in Table 5. Using the parameters derived by FOTEL, the fit to the RV curves is shown in Fig. 2 and to two of the photometric datasets in Fig. 3. Overall there is very good agreement although there appears to be a very small remaining systematic effect in the residuals in the fit to the B-lightcurve, albeit at a level well below 0.01 mag.

There is good agreement between the results obtained between FOTEL and PHOEBE and with results previously derived, which are summarised in Table 6. The largest difference is in the effective temperature of the secondary, where PHOEBE gives lower values. In addition, PHOEBE quotes much smaller internal error bars while error bars quoted by FOTEL are based on determination of the covariance matrix and appear more realistic.

The fitting of the disentangled spectra and the derivation of the effective temperatures requires the knowledge of the masses and radii, which can only be obtained from fitting the RV and LC, which needs the effective temperature. This implies that an iteration step needs to be performed, which turns out to be very fast. The second column in Table 5 represents the fit results when the primary effective temperature is initially fixed at 9750 K, as previously determined by S05. The derived masses and radii were the ones used in the fitting of the disentangled spectra using the MARCS code, which resulted in an adopted effective temperature of 9950 K. The third column in Table 5 represents the fit results when the primary effective temperature is now fixed to this value. The resulting parameters are barely changed, indicating that the exact effective temperature of the primary has only a very small influence on the derived parameters of the system.

[5] Explicitly: for (primary, secondary) values of (0.51, 0.65) at 3458 Å, (0.61, 0.69) at 4033 Å, (0.61, 0.68) at 4233 Å, (0.61, 0.68) at 4468 Å, (0.53, 0.58) at 5387 Å, (0.52, 0.58) at 5462 Å, (0.50, 0.58) at 5792 Å, (0.52, 0.58) at 5439 Å, (0.60, 0.67) at 4342 Å, and (0.52, 0.58) at 4600 Å are adopted.

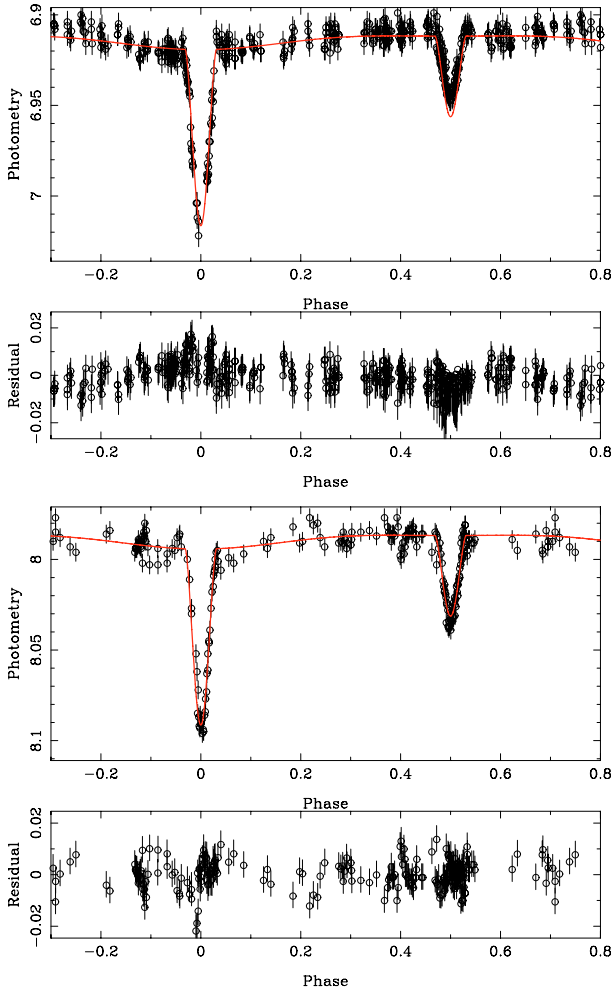

Fig. 3. Photometry and residuals for the B-band (from M04, *top panel*) and Geneva G (this paper, *bottom panel*).

5. The distance to HD 23642

Theoretical component and system magnitudes are calculated from the MARCS model atmospheres. A MARCS model of Vega with $T_{\rm eff}$ = 9650 K, $\log g$ = 3.95, [Fe/H] = −0.4), assuming no interstellar reddening, is used to determine the zero point fluxes in the relation:

$$m = -2.5 \log \left(\frac{\int (\lambda/\lambda_0)\, F_\lambda\, R_\lambda\, {\rm d}\lambda}{\int R_\lambda\, {\rm d}\lambda} \right) + m_0. \quad (3)$$

The response curves R_λ are taken from the "Asiago Database on Photometric Systems" (Moro & Munari 2000), and Vega is assumed to have $V = +0.03$, $B - V = 0.00$, $U - B = 0.00$ (in the Johnson system), $V = 0.061$, and $U, B, B1, B2, V1, G$ colours of, respectively, 1.505, 0.959, 0.900, 1.510, 1.662 and 2.168 (in the Geneva system), and $b - y = 0.003$, $m_1 = 0.157$, $c_1 = 1.088$ (in the Strömgren system).

The reddening to the Pleiades is variable. M04 derived for HD 23642 $E(B - V) = 0.011$ from the equivalent width of the interstellar Na I D-lines, while average values for the cluster reddening quoted in the literature are $E(B - V) = 0.057$ (from $E(b - y) = 0.04$, Crawford & Perry 1976), 0.059 (from $E(B2-V1) = 0.052$, Nicolet 1981) and $E(B-V) = 0.045 \pm 0.010$ (Soderblom et al. 2005). We investigated the strength of one of the strongest Diffuse Interstellar Band (DIB) at 5780 Å. A 3σ upper limit of 12 mÅ is derived, and comparison with the

Table 5. Results from the LC en RV fitting. The third column represents the final fit.

Variable	FOTEL	FOTEL	PHOEBE
P (d)	2.46113346 ± 0.00000069	2.46113346 ± 0.00000069	2.46113358 ± 0.00000015
$T_{0,\mathrm{prim.min.}}$ (HJD)	2 452 903.59904 ± 0.00051	2 452 903.59904 ± 0.00051	2 452 903.60002 ± 0.00014
a ($R_\odot$)	11.956 ± 0.022	11.954 ± 0.022	11.959 ± 0.0052
V_γ (km s^{-1})	5.42 ± 0.12	5.42 ± 0.12	5.39 ± 0.04
q	0.7045 ± 0.0026	0.7045 ± 0.0026	0.7054 ± 0.0006
i (deg)	77.55 ± 0.15	77.60 ± 0.15	76.63 ± 0.02
e	0.0 ± 0.002	0.0 ± 0.002	0.0 (fixed)
K_1 (K)	99.22 ± 0.29	99.22 ± 0.29	99.43 ± 0.07
K_2 (K)	140.83 ± 0.32	140.83 ± 0.32	140.96 ± 0.09
T_1 (K)	9750 (fixed)	9950 (fixed)	9950 (fixed)
T_2 (K)	7551 ± 39	7640 ± 40	7281 ± 9
(r_1/a)	0.1531 ± 0.0031	0.1542 ± 0.0031	0.15804 ± 0.00028
(r_2/a)	0.1344 ± 0.0035	0.1327 ± 0.0035	0.13128 ± 0.00026
R_1 ($R_\odot$)	1.830 ± 0.037	1.843 ± 0.037	1.890 ± 0.003
R_2 ($R_\odot$)	1.607 ± 0.042	1.586 ± 0.042	1.570 ± 0.003
M_1 ($M_\odot$)	2.222 ± 0.027	2.221 ± 0.027	2.230 ± 0.010
M_2 ($M_\odot$)	1.566 ± 0.015	1.565 ± 0.015	1.573 ± 0.002
$\log g_1$ (cgs)		4.253 ± 0.019	
$\log g_2$ (cgs)		4.231 ± 0.024	
$V_{\mathrm{rot},1}\ \sin i$ (km s^{-1})		36.5 ± 0.8	
$V_{\mathrm{rot},2}\ \sin i$ (km s^{-1})		31.9 ± 1.2	

Table 6. Parameters derived for the system HD 23642 from the literature.

Variable	Munari et al. (2004)	Southworth et al. (2005)	Torres (2003)
P (d)	2.46113400 ± 0.00000034		2.46113329 ± 0.00000066
T_0 (HJD)	2 452 903.5981 ± 0.0013		2 436 096.5204 ± 0.0040
V_γ (km s^{-1})	5.17 ± 0.24	6.07 ± 0.39	6.1 ± 1.7
q	0.6966 ± 0.0034	0.7068 ± 0.0050	0.6934 ± 0.0077
$a\ \sin i$ ($R_\odot$)	11.699 ± 0.030	11.636 ± 0.040	11.566 ± 0.061
i (deg)	78.10 ± 0.21	77.78 ± 0.17	∼78
a	11.956 ± 0.030	11.906 ± 0.041	∼11.82
e	0.0 ± 0.002		0 (adopted)
T_1 (K)	9671 (fixed)	9750 ± 250	
T_2 (K)	7500 ± 61	7600 ± 400	
R_1 ($R_\odot$)	1.81 ± 0.030	1.831 ± 0.029	
R_2 ($R_\odot$)	1.50 ± 0.026	1.548 ± 0.044	
M_1 ($M_\odot$)	2.24 ± 0.017	2.193 ± 0.022	
M_2 ($M_\odot$)	1.56 ± 0.014	1.550 ± 0.018	
$\log g_1$ (cgs)	4.27 ± 0.015	4.254 ± 0.014	
$\log g_2$ (cgs)	4.28 ± 0.016	4.249 ± 0.025	

recent work by Megier et al. (2005) then suggests a formal upper limit of 0.05 to $E(B-V)$.

The reddening law is taken from Cardelli et al. (1989) and O'Donnell (1994) and $R_\mathrm{V} = 3.1$ is adopted. The component magnitudes and the out-of-eclipse system magnitudes can be predicted for given $E(B-V)$, distance and stellar radii, and the interpolated MARCS models for the given effective temperatures, gravities and metallicity. The out-of-eclipse system magnitudes can then be compared to observations (see Table 7). For the Geneva and B, V colours they are the observed out-of-eclipse magnitudes with rms errors as they come out of the LC fitting. Also listed are the 2MASS JHK magnitudes (taken at JD = 2 451 138.7117 and therefore are taken out-of-eclipse), and the mean Strömgren V, $b-y$, m_1, and c_1 colours taken from Crawford & Perry (1976), as listed in the WEBDA database[6]. A χ^2 can be defined as

$$\chi^2_\mathrm{m} = \sum (m_\mathrm{model} - m_\mathrm{observed})^2 / (\sigma^2_\mathrm{model} + \sigma^2_\mathrm{observed}) \quad (4)$$

where the sum includes the 7 Geneva magnitudes, Johnson B and V, and the 3 Strömgren colours. m_model depends on $E(B-V)$, distance, T_1, T_2, R_1, R_2, and Z. The 2MASS magnitudes are not included in the sum, as the MARCS model atmospheres are only calculated up to 7000 Å. As a test, however, the model atmospheres have been extended into the IR by a black-body extrapolation in order to be able to predict IR magnitudes. The value for σ includes the rms errors listed in Table 7 as well as a general calibration error due to the uncertainties in determining the zero points, and is assumed to be 0.004 mag for the Strömgren colours and 0.006 for the 7 Geneva and Johnson B and V magnitudes. These numbers are realistic in itself, but have also been chosen in order to give a reduced χ^2 near unity for the overall best fit.

Another method to determine the distance is to use the SB technique, which related the angular diameter (θ in units of milli-arcseconds) to a photometric colour. This was advocated specifically for B-stars using the Strömgren c_1-index, or Geneva d-index by Salaris & Groenewegen (2002). S05 have used the SB-technique on HD 23642 using empirical relations with

[6] see `http://obswww.unige.ch/webda/cgi-bin/frame_list.cgi?mel022/`, HD 23642 is listed as star number 1431.

Table 7. Model predicted component (m_1, m_2) and system magnitudes ($m_{\rm model}$) and the observed out-of-eclipse magnitudes.

Colour	m_1	m_2	$m_{\rm model}$	$m_{\rm observed}$
model **A:**	9950/7640/+0.06 ; 1.843/1.586 ; 0.020/137.9			
v	7.126	8.296	6.808	6.819 ± 0.0049
u	7.610	9.140	7.373	7.370 ± 0.0070
$b1$	7.085	8.616	6.848	6.846 ± 0.0053
b	6.179	7.648	5.929	5.946 ± 0.0053
$b2$	7.687	9.069	7.419	7.425 ± 0.0051
$v1$	7.832	9.031	7.521	7.521 ± 0.0055
g	8.331	9.451	8.000	7.992 ± 0.0057
$B_{\rm J}$	7.110	8.523	6.848	6.916 ± 0.0054
$V_{\rm J}$	7.096	8.274	6.780	6.840 ± 0.0036
$(B-V)_{\rm J}$	0.014	0.249	0.068	0.076 ± 0.0065
J	7.022	7.769	6.580	6.635 ± 0.023
H	6.979	7.652	6.507	6.641 ± 0.026
K	6.962	7.598	6.482	6.607 ± 0.024
$V_{\rm Str}$	7.244	8.763	7.004	6.800 ± 0.015
$(b-y)$	0.010	0.146	0.043	0.041 ± 0.003
m_1	0.158	0.226	0.169	0.163 ± 0.002
c_1	1.015	0.808	0.971	0.930 ± 0.005
model **B:**	10100/7590/+0.06 ; 1.843/1.670 ; 0.025/140.2			
v	7.143	8.262	6.811	6.819 ± 0.0049
u	7.609	9.118	7.368	7.370 ± 0.0070
$b1$	7.092	8.598	6.850	6.846 ± 0.0053
b	6.190	7.628	5.934	5.946 ± 0.0053
$b2$	7.701	9.046	7.425	7.425 ± 0.0051
$v1$	7.848	8.999	7.525	7.521 ± 0.0055
g	8.348	9.414	8.002	7.992 ± 0.0057
$B_{\rm J}$	7.122	8.501	6.854	6.916 ± 0.0054
$V_{\rm J}$	7.112	8.240	6.783	6.840 ± 0.0036
$(B-V)_{\rm J}$	0.010	0.261	0.071	0.076 ± 0.0065
J	7.043	7.710	6.574	6.635 ± 0.023
H	6.994	7.589	6.499	6.641 ± 0.026
K	6.986	7.533	6.473	6.607 ± 0.024
$V_{\rm Str}$	7.255	8.745	7.010	6.800 ± 0.015
$(b-y)$	0.011	0.155	0.047	0.041 ± 0.003
m_1	0.153	0.225	0.164	0.163 ± 0.002
c_1	1.008	0.796	0.961	0.930 ± 0.005

The model parameters are listed as $T_1/T_2/[Fe/H]$; R_1/R_2; $E(B-V)/d$. JHK magnitudes are only given for reference as in that wavelength range the model atmospheres were extrapolated using a blackbody.

effective temperature and traditional colours like $(B-V)$. Specifically, one has, (see, e.g. Groenewegen 2004):

$$\theta_{(m_\lambda=0)} = \theta_{\rm model}\ 10^{m_\lambda/5} \quad (5)$$

with the following calibrated relations:

$$\theta_{(V=0)} = 1.824\ c_1 + 1.294 \qquad \text{rms} = 0.097, \quad (6)$$

$$\log\theta_{(V=0)} = 0.274\ (V-K)_0 + 0.519 \qquad \text{rms} = 0.022, \quad (7)$$

and

$$\log\theta_{(V=0)} = 0.725\ (B-V)_0 + 0.492 \qquad \text{rms} = 0.047. \quad (8)$$

The calibrations come from Salaris & Groenewegen (2002) for the c_1 index, and from Groenewegen (2004) for $(V-K)$ and $(B-V)$[7]. The latter two relations are in good agreement with the ones quoted by Kervella et al. (2004).

One can define a χ^2 like

$$\chi^2_\theta = \sum(\theta_{\rm model} - \theta_{\rm obs})^2/(\sigma^2_{\rm model} + \sigma^2_{\rm obs}) \quad (9)$$

[7] The latter relation was not quoted in that paper, but has been derived for dwarfs and subgiants based on the same dataset.

where the sum includes the angular diameter derived from the c_1 SB calibration for the primary, and the $(B-V)$ calibration for primary and secondary. $\theta_{\rm obs}$ and $\sigma_{\rm obs}$ are derived from R/d (radius/distance) and the error in R, while $\sigma_{\rm model}$ represents the rms error in the SB calibration itself. The SB technique can not be applied using the Geneva d-index nor for the secondary using the c_1 index as the colours are outside the range for which the calibrations are valid. For the reasons given above, the angular diameter for primary and secondary based on the $(V-K)$ calibration have been calculated but are not included in the sum.

For the standard model ([Fe/H] = +0.06 dex, effective temperatures from Table 4, radii from Table 5) the distance that best fits the photometry is correlated with the adopted reddening and equals 140.4 pc (for $E(B-V) = 0.010$), 139.2 pc (for $E(B-V) = 0.015$) to 134.4 pc (for $E(B-V) = 0.035$). For the standard model, the best absolute fit to the photometry is obtained with $E(B-V) = 0.020$ and 137.9 pc. For that model, the predicted magnitudes are listed in Table 7 and the predicted angular diameters are given in Table 8 as model A, where they are compared to the observations. The agreement is excellent in the Geneva colours and rather poor in Johnsons B, V and the Strömgren c_1-index. In fact, the fitting was done excluding these three colours. Including them would lead to an overall worse best fit (from a reduced χ^2 of 1.29 to 13.0), but very similar best fit values of $E(B-V) = 0.015$ and 140.2 pc.

Better fits may be obtained by varying the parameters within the error bars. A grid of model spectra was generated varying T_1 and T_2 in steps of 50 K, R_1 and R_2 in steps of their respective $\frac{1}{2}\sigma$ error bars, Z ([Fe/H] = 0, +0.06, +0.12), as well as $E(B-V)$ (0.015, 0.020, 0.025, 0.030) and distance (steps of 0.5 pc).

The best fit ($\chi^2 = 0.84$) is obtained for $T_1 = 10\,100 \pm 35$ K, $T_2 = 7590 \pm 55$ K, $R_1 = 1.843 \pm 0.009$, $R_2 = 1.670 \pm 0.025$, [Fe/H] = +0.06 ± 0.23, $E(B-V) = 0.025 \pm 0.002$, $d = 140.2 \pm 0.6$ pc. The error bars have been estimated by changing one parameter at a time until a χ^2 of $\chi^2_{\rm min} + 1$ is reached. The predicted magnitudes are listed in Table 7 and the predicted angular diameters in Table 8 as model B. Both for primary and secondary component the predicted angular diameters are in very good agreement with those predicted by the SB technique (expect those based on $(V-K)$, for reasons already explained).

The formal errors in the parameters are very (unrealistically) small and this is due to the interdependence of the parameters. For example changing the effective temperature of a component (without changing the distance) will lead to a larger luminosity which will lead to a change of all magnitudes by quite an amount. To get a better feeling for the true uncertainties, in particular for the reddening and distance, the 20 best solutions (with $\chi^2 < 0.87$) were inspected. All these models have a reddening of either 0.020 or 0.025, and the distances range between 132.8 and 140.2 pc.

Again, these results do no change significantly when the Johnson B, V and Strömgren c_1-index are included in the fit.

Based on these consideration a reddening of $E(B-V) = 0.025 \pm 0.003$ and distance of $d = 138.0 \pm 1.5$ pc to HD 23642 are adopted as our best estimates.

6. Comparison to evolutionary models

Radius and mass distribution predicted by scaled solar isochrones with and without convective core overshoot have been compared to the values obtained from the binary analysis (data from Col. 3 of Table 5). We used isochrones from Pietrinferni et al. (2004) for [Fe/H] = +0.058 and a reference age of 130 Myr, consistent with recent estimates by

Table 8. Observed and predicted angular diameters.

Model	$\theta_{\rm pred,1}$	$\theta_{\rm SB,c_1,1}$	$\theta_{\rm SB,(B-V),1}$	$\theta_{\rm SB,(V-K),1}$	$\theta_{\rm pred,2}$	$\theta_{\rm SB,(B-V),2}$	$\theta_{\rm SB,(V-K),2}$
A: 9950/7640/+0.06; 1.843/1.586; 0.020/137.9	0.124 ± 0.002	0.123	0.120	0.136	0.107 ± 0.003	0.104	0.111
B: 10100/7590/+0.06; 1.843/1.670; 0.025/140.2	0.122 ± 0.002	0.122	0.119	0.134	0.111 ± 0.003	0.107	0.115

The model parameters are listed as T_1/T_2/[Fe/H]; R_1/R_2; $E(B-V)/d$. Predicted angular diameters are calculated from $2R_{1,2}/D$. Observed angular diameters are given for different SB relations. The two based on $(V-K)$ are only given for reference as in that wavelength range the model atmospheres were extrapolated using a blackbody.

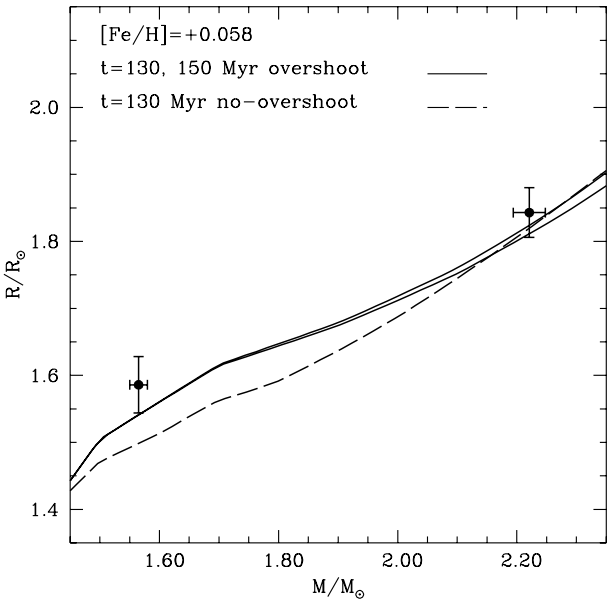

Fig. 4. Radius and mass distribution along [Fe/H] = +0.058 scaled solar isochrones for 130 and 150 Myr including mild overshoot (solid lines – the older isochrone is the one showing larger radii at a given mass) and for a 130 Myr isochrone without overshoot (dashed line; all isochrones from Pietrinferni et al. 2004) are compared with the corresponding values obtained for the two components of HD 23642.

Stauffer et al. (1998, 125−130 Myr) and Castellani et al. (2002, 130 Myr). An age of 150 Myr is also displayed to highlight the effect of an age change on the radius-mass diagram.

Figure 4 shows the result of this comparison. Isochrones with convective overshoot are able to fit simultaneously both components, within the 1σ error-boxes. Models without convective overshoot fail, given that the secondary component cannot be matched by the theoretical isochrone at the Pleiades age. Changing the age around the 130 Myr value would not improve the fit, because this component lies on the unevolved part of the isochrone Main Sequence, even if the age is increased up to unrealistically high ages of 200−250 Myr (moreover, in case of such high ages, isochrones would not be able to match the primary component).

If the [Fe/H] of the system is kept fixed at the standard value of [Fe/H] = 0.06, a slight increase of the core overshoot extension in the theoretical isochrones coupled to an age of 150−160 Myr would improve further the fit to the radii of the system components.

7. Summary and discussion

New data on the only known eclipsing binary in the Pleiades are presented: 11 new radial velocities and 211 7-band photometric data points in the Geneva system. The high resolution spectra are disentangled with the KOREL code. The resulting component spectra are fitted with model atmospheres generated with the MARCS code. The temperature of the primary is about 10 000 K and that of the secondary 7600 K, depending slightly on metallicity. The temperature of the primary is slightly warmer than adopted by M04 and S05, and the temperature of the secondary is in good agreement with those earlier results.

The new data are combined with published radial velocity and photometric data and analysed with the FOTEL and PHOEBE codes. Masses and radii are derived with 1% and 2−3% accuracy and agree within the respective 1σ error bars with the previous results of M04 and S05.

By fitting the MARCS model atmospheres (as a function of effective temperature, radius and metallicity) to the observed out-of-eclipse magnitudes, a best fit is obtained for $E(B-V) = 0.025 \pm 0.003$ and distance of $d = 138.0 \pm 1.5$ pc. This is in between the values found by M04 (132 ± 2 pc) and S05 (139.1 ± 3.5 pc).

Munari et al. (2004) find a lower reddening of $E(B-V) = 0.012 \pm 0.004$, based on a very similar method to ours, which is also adopted by S05. For the reddening adopted in the present paper, the distance derived in the other 2 papers would become shorter by about 3 pc. In this respect, our results agree best with those in S05.

The distance is confirmed by independently considering the angular diameter of both components derived directly from the observed radii (for a given distance) with those derived from several SB relations (which depend on the predicted colours of the components).

Table 9 lists recent distance estimates to the Pleiades starting with the ones based on the Hipparcos trigonometric parallax and ending with the three distance estimates to HD 23642. These three estimates agree within each others error bars, especially when the revised distance by S05 to the M04 value is considered. These distances also agree with recent independent estimates using various methods. One should remark that M04 and S05 assume slightly different reddenings, and when considering that, the distance derived in the present paper is slightly longer than the other two (but not significantly so). This is likely due to the slightly higher primary effective temperature derived here.

For the distance estimates based on an individual object (HD 23850 and HD 23642) one also has to consider the depth of the cluster. Estimates for the (1-sigma) dispersion in distance along the line-of-sight are of order 3−4 pc (Soderblom et al. 2005; Narayanan & Gould 1999) based on the dispersion of the parallaxes and proper motions. A core radius of $5.0^{+3.0}_{-1.5}$ pc has been determined from the brown dwarf distribution (Jameson et al. 2002). Based on this one may conclude that there is no evidence that HD 23642 is significantly in front or behind the centre of the cluster.

Finally, radii and masses derived from the binary analysis are compared to the mass and radius distribution along the theoretical isochrones by Pietrinferni et al. (2004), at the Pleiades' age.

Table 9. Various recent distance estimates to the Pleiades.

Method	Reference	Distance (pc)
Hipparcos trigonometric parallax	van Leeuwen & Hansen Ruiz (1997)	116.1 ± 3.0
Hipparcos trigonometric parallax	van Leeuwen (1999)	118.3 ± 3.4
Ground-based trigonometric parallaxes	Gatewood et al. (2000)	130.9 ± 7.0
Hipparcos proper motions + RV data	Narayanan & Gould (1999)	130.7 ± 11.1
Hipparcos proper motions + RV data	Li & Junlian (1999)	135.6 ± 0.7
Hipparcos Intermediate Astrometry Data	Makarov (2002)	129.0 ± 3.2
Infra-red Main-Sequence fitting	Percival et al. (2005)	133.8 ± 3.9
Astrometric binary HD 23850	Zwahlen et al. (2004)	132 ± 4
HST parallaxes of three Pleiades stars	Soderblom et al. (2005)	134.6 ± 3.1
Eclipsing binary HD 23642	Munari et al. (2004)	131.9 ± 2.1[a]
Eclipsing binary HD 23642	Southworth et al. (2005)	139.1 ± 3.5
Eclipsing binary HD 23642	this work	138.0 ± 1.5

[a] Southworth et al. (2005) suggest that this should be corrected to 135.5 ± 2.3 pc because they claim there is an inconsistency between the Solar luminosity and absolute magnitude adopted in the WD-code and in the BCs adopted by Munari et al.

Isochrones including convective core overshoot[8] reproduce simultaneously the mass-radius values obtained for the two components, within the corresponding 1σ error bars. Models without convective core overshoot fail to do so.

Is there room for improvement? The question of distance seems to be settled, in particular with respect to the question of the Hipparcos distance. Table 7 does reveal a discrepancy of order 5σ in the infrared. Whether this discrepancy is significant or not is difficult to judge. First of all the MARCS models were extrapolated as blackbodies beyond 7000 Å, and on the other hand the 2MASS magnitudes may not be 100% reliable at this very bright level. A lightcurve and a spectrum at quadrature in the infrared might therefore be useful for several reasons. An infrared spectrum might further constrain the effective temperature, while an out-of-eclipse IR magnitude would further constrain the reddening estimate and/or the estimate of R_V.

Acknowledgements. The authors would like to thank Petr Harmanec (Ondřejov Observatory) for his comments on a draft version and for very stimulating discussion regarding the use of FOTEL and KOREL. His three month visit to our institute in 2003 was paramount in this respect. The author of both codes, Petr Hadrava (Ondřejov Observatory), also provided valuable feedback. The authors would also like to thank Jadwiga Daszynska (Wroclaw University), Joris De Ridder, N. Cramer (Geneva Observatory), Thomas Maas, Pierre-Olivier Bourge (Ulg), Hans Van Winckel and Wim De Meester for taking the MERCATOR photometric data, and Pieter Deroo and Anwesh Mazumdar for taking part of the CORALIE spectroscopic data, Sue Percival and Daniel Brown for valuable discussions. This research has made use of the SIMBAD database, operated at CDS, Strasbourg, France. L.D. acknowledges financial support from the Fund for Scientific Research, Flanders (FWO), Belgium.

References

Abt, H. A. 1958, ApJ, 128, 139
Abt, H. A., & Levato, H. 1978, PASP, 90, 201
Baranne, A., Queloz, D., Mayor, M., et al. 1996, A&AS, 119, 373
Boesgaard, A. M. 2005, in Cosmic Abundances as records of Stellar Evolution and Nucleosynthesis, ed. T. G. Barnes III, & F. N. Bash., ASPC 336, 39
Boesgaard, A. M., & Friel, E. D. 1990, ApJ, 351, 467
Cardelli, J. A., Clayton, G. C., & Mathis, J. S. 1989, ApJ, 345, 245
Castellani, V., Degl'Innocenti, S., Prada Moroni, P. G., & Tordiglione, V. 2002, MNRAS, 334, 193
Claret, A. 2000, A&A, 363, 1081
Claret, A. 2003, A&A, 401, 657
Crawford, D. L., & Perry, C. L. 1976, AJ, 81, 419
Decin, L., Waelkens, C., Eriksson, K., et al. 2000, A&A, 364, 137
Decin, L., Shkedy, Z., Molenberghs, G., Aerts, M., & Aerts, C. 2004, A&A, 421, 281
Edvardsson, B., Andersen, J., Gustafsson, B., et al. 1993, A&A, 275, 101
Etzel P. B. 1975, Masters Thesis, San Diego State Univ.
Etzel, P. B. 1981, in Photometric and Spectroscopic Binary Systems, ed. E. B. Carling, & Z. Kopal, NATO ASI Ser. C., 69 (Dordrecht: Kluwer), 111
Fitzpatrick, E. L., & Massa, D. 2005, AJ, 129, 1642
Gatewood, G., de Jonge, J. K., & Han, I. 2000, ApJ, 533, 938
Giannuzzi, M. A. 1995, A&A, 293, 360
Griffin, R. F. 1995, JRASC, 89, 53
Groenewegen, M. A. T. 2004, MNRAS, 353, 903
Gustafsson, B., Bell, R. A., Eriksson, K., & Nordlund, Å 1975, A&A, 42, 407
Hadrava, P. 1990, Contrib. Astron. Obs. Skal. Pl., 20, 23
Hadrava, P. 1995, A&AS, 114, 393
Hadrava, P. 2004a, Publ. Astron. Inst. Acad. Sci., 92, 1
Hadrava, P. 2004b, Publ. Astron. Inst. Acad. Sci., 92, 15
Jameson, R. F., Dobbie, P. D., Hodgkin, S. T., & Pinfield, D. J. 2002, MNRAS, 335, 853
Jørgensen, U. G., Johnson, H. R., & Nordlund, Å 1992, A&A, 261, 263
Kervella, P., Thévenin, F., Di Folco, E., & Ségransan, D. 2004, A&A, 426, 297
King, J. R., Soderblom, D. R., Fischer, D., & Jones, B. F. 2000, ApJ, 533, 944
Li, C., & Junlian, Z. 1999, ASPC, 167, 259
Makarov, V. 2002, AJ, 124, 3299
Megier, A., Krelowski, J., & Weselak, T. 2005, MNRAS, 358, 563
Moro, D., & Munari, U. 2000, A&AS, 147, 361 (see database at: `http://ulisse.pd.astro.it/Astro/ADPS/`)
Munari, U., Dallaporta, S., Siviero, A., et al. 2004, A&A, 418, L31 (M04)
Narayanan, V. K., & Gould, A. 1999, ApJ, 523, 328
Nicolet, B. 1981, A&A, 104, 585
O'Donnell, J. E. 1994, ApJ, 422, 158
Pearce, J. A. 1957, Publ. Dom. Astr. Obs., 10, 435
Percival, S. M., Salaris, M., & Groenewegen, M. A. T. 2005, A&A, 429, 887
Pietrinferni, A., Cassisi, S., Salaris, M., & Castelli, F. 2004, ApJ, 612, 168
Plez, B., Brett, J. M., & Nordlund, Å 1992, A&A, 256, 551
Popper, D. M., & Etzel, P. B. 1981, AJ, 86, 102
Press, W. H., Teukolsky, S. A., Vetterling, W. T., & Flannery, B. P. 1992, in Numerical Recipes in Fortran 77 (Cambridge UP)
Prša, A., & Zwitter, T. 2005, ApJ, 628, 426
Rufener, F. 1988, in Catalogue of stars measured in the Geneva observatory photometric system, fourth edition, Observatoir de Genève
Salaris, M., & Groenewegen, M. A. T. 2002, A&A, 381, 440
Soderblom, D. R., Nelan, E., Fritz Benedict, G., et al. 2005, AJ, 129, 1616
Southworth, J., Maxted, P. F. L., & Smalley, B. 2005, A&A, 429, 645 (S05)
Southworth, J., Smalley, B., Maxted, P. F. L., & Etzel, P. B. 2004, The A-star puzzle, ed. J. Zverk, W. W. Weiss, J. Ziznovsky, & S. J. Adelman (Cambridge UP), in IAU Symp., 224, 548
Stauffer, J. R., Schultz, G., & Kirkpatrick, J. D. 1998, ApJ, 499, L199
Torres, G. 2003, IBVS, 5402, 1
van Leeuwen, F., & Hansen Ruiz, C. S. 1997, ESA SP-402, 689
van Leeuwen, F. 1999, A&A, 341, L71
Wilson, R. E., & Devinney, E. J. 1971, AJ, 166, 605
Zwahlen, N., North, P., Debernardi, Y., et al. 2004, A&A, 425, L25

[8] At a level of 0.2 of the local pressure scale height.